Supporting Information

Ozonation of *para*-substituted phenolic compounds yields *p*-benzoquinones, other cyclic α, β -unsaturated ketones, and substituted catechols

Peter R. Tentscher[†], *Marc Bourgin*[†], *Urs von Gunten*[†,‡,*]

[†] Eawag, Swiss Federal Institute of Aquatic Science and Technology, Ueberlandstrasse 133, 8600 Duebendorf, Switzerland

[‡]School of Architecture, Civil and Environmental Engineering (ENAC), École Polytechnique Fédérale de Lausanne (EPFL), 1015, Lausanne, Switzerland

*Corresponding author

phone: +41 58 765 5270, fax:+41 58 765 5802, email: vongunten@eawag.ch

and (b) standard mix, 3D chromatograms of (c) sample and (d) standard mix, UV/Vis spectrum at a retention time of 4.2 min of (e) sample and (f) standard mix, MS/MS mass spectra of this peak of (g) sample and (h) standard.

Table S2: Properties of HRMS peaks with deuterated *p*-methylphenol. Ring deuteration refers to aromatic deuterons (+4 d in the parent), methyl deuteration to the *p*-methyl-group (+3 d in the parent)

Section S3. Identification of 4-methyl-*o*-benzoquinone

Figure S3: Left: HPLC-DAD chromatograms of *p*-methylphenol and *p*-methylcatechol reaction mixtures with ozone and HOCl as oxidants. Middle: UV/Vis spectra at a retention time of 3.7 min. Right: Zoom on the region around 400 nm.

Section S4. Hydroquinone formation in the *p*-methoxyphenol reaction mixture

Figure S4: HPLC-DAD chromatogram of a mixture of *p*-methoxycatechol and *p*-benzoquinone (mix of 100 µM solution in phosphate buffer, pH 7). Extracted UV/Vis spectra of known components and presumed *p*-methoxy-*o*-benzoquinone.

Section S5. Expected post-ozonation dynamics in the presence of nucleophiles

Figure S5: Examples of expected reactions of primary products of ozonation of (substituted) phenols. In biological media (e.g. inside cells), nucleophiles in addition to hydroxide are present (amino groups of amino acids, thiol groups of cysteine moieties of enzymes).

Section S6. Product yield as a function of specific ozone dose

Figure S6.1: Product yields as a function of specific ozone dose for unsubstituted phenol. Different colors refer to different experimental series (see above). Empty plots indicate that no catechol was detected.

FigureS6.2: Product yields as a function of specific ozone dose for *p*-methylphenol.

Figure S6.3: Product yields as a function of specific ozone dose for *p*-ethylphenol.

Figure S6.4: Product yields as a function of specific ozone dose for *p*-isopropylphenol.

Figure S6.5: Product yields as a function of specific ozone dose for *p*-*tert*-butylphenol.

Figure S6.6: Product yields as a function of specific ozone dose for *p*-methoxyphenol.

Figure S6.7: Product yields as a function of specific ozone dose for *p*-chlorophenol.

Figure S6.8: Product yields as a function of specific ozone dose for *p*-bromophenol.

Figure S6.9: Product yields as a function of specific ozone dose for *p*-formylphenol.

Figure S6.10: Product yields as a function of specific ozone dose for *p*-carboxyphenol.

Figure S6.11: Product yields as a function of specific ozone dose for 2,6-dimethylphenol.

Figure S6.12: Product yields as a function of specific ozone dose for 2,6-dibromophenol. 3-bromocatechol was not unambiguously identified, owing to overlapping peaks. Given yields are best estimates assuming the correct identity of the transformation product.

Section S7. Mechanistic discussion

Figure S7.1: Evaluated reaction pathways for neutral phenol. Reported energies are Gibbs free energies (kcal/mol) with respect to separate molecules of ozone and phenol. IRC calculations for transition structures leading to the cyclic ozonide and to the trioxo-species were not successful, presumably because the potential energy surfaces are very flat in these regions.

Figure S7.2: Proposed formation pathways of hydroquinone in the reaction mixtures of *p*-tert-butylphenol and *p*-methoxyphenol. Free energies from CBS-QB3 gas phase calculations and SMD implicit solvation energies. Free energies for the S_N1 reaction vary depending on the inclusion of explicit water molecules (not shown).

S0. Materials and Methodology

S0.1 Compounds

Purchased organic compounds are listed in Table S1. *p*-benzoquinone was further purified by sublimation and the remaining hydroquinone content was corrected for, quantifying hydroquinone by HPLC-DAD (see below). All other compounds were used as received. 4-hydroxy,4'-methylcyclohexadienone and 4-hydroxy,4'-ethylcyclohexadienone were synthesized from *p*-methylphenol and *p*-ethylphenol with oxone as the oxidant [1]. They were purified with flash chromatography, and the purity was estimated from the HPLC-DAD peak areas at 200 nm. Ultrapurified water produced by a "barnstead nanopure" system from Thermo Scientific was used for the preparation of all solutions. Organic solvents were HPLC grade.

S0.2 Ozonation batch experiments

Experiments were performed as follows: phenol stock solutions (0.05-0.1 M) were freshly prepared in a 50% (5.2 M) tertiary-butanol (*t*-BuOH) solution. 400 mL of 5 mM phosphate buffer (pH 3.0, pH 7.0) was spiked with 400-800 µL phenolic stock (final phenol concentration 99 µM) and 5 mL 50% *t*-BuOH ($^{\cdot}OH$ scavenger, final concentration 65 mM). The ozone stock solution was prepared by bubbling ozone from an oxygen-fed ozone generator (CMG 3-3, Apaco AG, Switzerland) through room-temperature nanopure water. The concentrations, ~500-700 µM, were determined photometrically (ε (260 nm) = 3200 $M^{-1}cm^{-1}$) [2].

50 mL of phenol solutions were stirred in a 100 mL beaker at room temperature (22±2 ^{o}C), different volumes (1, 2, 5, 10 mL) of room temperature O_3 stock solution (~500-700 µM) were added and the mixture was stirred for another 10 s. This corresponds to molar ratios of O_3 to substrate of ~0.125 to ~1.75, which resulted in immediate complete depletion of O_3 because of the high second order rate constants for the reactions of ozone with the selected phenolic compounds [2]. Within a series, duplicate experiments were performed for the lowest three O_3 doses. An experimental series was completed within 20 min. Reaction mixtures at pH 7 were acidified with 150 µL of 42.5% H_3PO_4 directly thereafter, yielding a pH <3. This was done to prevent hydrolysis of *p*-benzoquinones and autooxidation of hydroquinones and catechols, which are strongly pH-dependent reactions. Samples were stored in the dark at 4 °C prior to analysis by HPLC-DAD within 24 h.

To determine the yield of H_2O_2 during the ozonation of phenol, *p*-chlorophenol, *p*-methylphenol, and *p*-methoxyphenol, experiments were performed as follows: phenol stock solutions (0.025 M) were prepared in 10% *t*-BuOH. 30 mL of 5 mM phosphate buffer (pH 3, pH 7) containing 209 mM *t*-BuOH were spiked with ~450 µL of a phenol stock to yield a phenol concentration of 400 µM. Varying volumes of the O_3 stock solution at room temperature (~700 µM) were added, yielding a total volume of ~10 mL; the solution was stirred for another 10 s. The H_2O_2 yield in unaltered samples was measured within 4 h (see below). For quantification of phenol abatement and product yields by HPLC, reaction mixtures were diluted 1:2 in 0.1275% H_3PO_4 and were stored in the dark at 4 °C prior to the analysis within 24 h.

The reaction of O_3 with H_2O_2 is too slow to interfere with the quantification of H_2O_2 or with the reaction of O_3 with the target phenols. The highest measurements of the rate constants of H_2O_2 and HO_2^- with O_3 are approximately 6.3×10^{-3} and 9.6×10^{6} $M^{-1}s^{-1}$, respectively, with a pK_a of H_2O_2 of 11.6-11.8. This results in apparent second order rate constants (k_{obs}) of 2.4×10^{2} $M^{-1}s^{-1}$ (pH 7) and 6.5×10^{-3} $M^{-1}s^{-1}$ (pH 3). k_{obs} for the reaction of O_3 with phenols (Table 1) are more than three orders of magnitude higher.

S0.3 Analytical methods

HPLC-DAD

Compounds were separated on a Cosmosil 5C18-MS-II (3.0x100 mm) HPLC column at 30 °C with a flux of 600 µL/min. Isocratic conditions (10% MeOH, 90% H_2O or 90% 0.1% H_3PO_4) were maintained for 4 min, then the MeOH concentration was increased to 50% or 75% with a gradient of 13%/min, depending on the compound. Injection volumes were 40-100 µL. Samples at neutral pH were acidified (see section S0.2).

HRMS

An aliquot (20 µL) was loaded on to the HPLC system and separated in a Cosmosil 5C18-MS-II (3.0x100 mm) HPLC column at 30 °C with a flux of 600 µL/min, using two eluents: (A) ultrapure water + 0.1% formic acid, and (B) methanol + 0.1% formic acid. Organic solvents were all LC-MS analysis grade from Merck. Initially, the proportion of eluent (A) remained constant at 90% during 4 min, decreased linearly to 25% between 4 min and 9 min and stayed at 25% over 4 min, and decreased again to 5% from 13.1 to 15 min, before going to the initial conditions for re-equilibration between 15.1 and 21 min.

After separation, the compounds were detected with a ThermoScientific Q-Exactive high resolution mass spectrometer. MS data were collected in full scan mode (m/z 60-700) at 70,000 resolution, using electrospray ionization, simultaneously in positive and negative mode.

Phosphate present in the reaction mixtures should not interfere with MS detection. Phosphate is ionized in the eluent (formic acid) and is not retained on the used column. A diversion valve was used to prevent the injection of ionic compounds (first seconds on chromatographic run) into the MS source.

Standards

Stock solutions of analytes were freshly prepared in MeOH and were stored in the dark at 4 °C until being used within 3 days of preparation. No increase in autooxidation products was observed in the stock solutions within this timespan, although many standards do contain detectable impurities (e.g. *p*-benzoquinone in hydroquinone standards and vice versa). External HPLC standards were prepared in 0.1% H_3PO_4 to prevent autooxidation of electron-rich hydroquinones and catechols, and to prevent reductive hydrolysis by hydroxide ions. No significant change in peak areas of standards was observed over the timespan of the analyses (usually completed within 48 h of the experiment).

Quantification of H_2O_2

10 mM HOCl was prepared in 100 mM phosphate buffer at pH 7 from a 1.94 M HOCl solution and standardized spectrophotometrically (ε(290 nm) = 350 $M^{-1}cm^{-1}$) [3]. 1 mL of the 10 mM HOCl solution was placed in a 1 cm quartz cuvette, and 1 mL unaltered sample was added with a Hamilton syringe. $^1O_2$ was detected by its phosphorescence at 1270 nm with a near infrared photomultiplier tube (Hamamatsu NIR-PMT H10330B-45, threshold level 200 mV, gate time 5 ms). All samples, prepared in duplicate, were measured as triplicates. External H_2O_2 standards prepared from a 10 mM stock solution standardized spectrophotometrically (ε(240 nm) = 40 $M^{-1}cm^{-1}$) [4], were prepared in phosphate buffer with *t*-BuOH and were measured as pentuplicates. The limit of quantification was ~3 µM. Attempts to measure H_2O_2 yields with the DPD method [5] or other photometric methods proved to be unsuitable, as (substituted) polyphenols produced during ozonation interfere with the detection, presumably by reducing the $DPD^{\cdot+}$ radical back to DPD.

S0.4 Quantum chemical calculations

Reaction pathway calculations of ozone addition to phenols were evaluated at the M062x/6-311+G(2d,2p)//M062x/may-cc-pVDZ [6-10] level of theory, employing the solute electron density (SMD) implicit solvation [11] model and a Grimme dispersion correction [12]. Selected results were checked against wB97XD/6-311+G(2d,2p) [13], which yielded comparable results. Yamaguchi's approximate spin projection method [14] was employed for O_3, $^1O_2$, and complexes of these species. The (uncorrected) high-spin potential energy surface was used for structures and vibrational frequencies. In cases where the nature of the transition structures was not obvious from visual inspection of the imaginary frequency, intrinsic reaction coordinate (IRC) [15] calculations were employed to ensure that transition structures connect reactants and products.

Free energies referring to complexes are indicated by using square brackets in the reaction schemes (Figures 3&4 (main text) and Figure S7.1). For example, reaction (B) in Figure 3 refers to the activated complex in the energy of the transition structure, but to separated molecules on the product side.

Protonation reactions were modeled as the reaction of a separate molecule of H_3O^+ with the anionic species, resulting in the neutral species and a separate molecule of H_2O. Although this is not very accurate energetically and cannot be used for the estimation of pK_a values, it is clear that protonation of the depicted alcoholates is energetically downhill.

Two reactions were modeled as catalyzed by two water molecules, indicated by "+2 H_2O / -2 H_2O" on the reaction arrow. The reported energies refer to the following: on the reactant and product side, energies of the bare molecules (no explicit water molecules) are reported. The activation barrier is computed as the difference between the transition structure and the pre-reactive complex, both including explicit water molecules. This energy difference is added to the ΔG value of the reactants in order to get $\Delta G(TS)$.

Generally, the reaction reported include many conformers, which are close (~2-3 kcal/mol) in energy. The reported energies always refer to the conformers lowest in energies or to the conformers which exhibited the lowest activation barriers for $\Delta G(TS)$.

QSAR descriptors for the estimation of rate constants and pK_a values used the M11/6-311+G(2d,2p)//M05/6-31+G(d)[16] model with SMD implicit solvation. The regression

model for rate constant calculations was adapted from the literature [17], although we used vertical ionization energies instead of orbital energies as descriptors. The regression models are described in more detail below (section S1.1).

Thermodynamic calculations on post-ozonation reactions (redox reactions and hydrolysis) applied a mix of different methods to get an accurate estimate of the free energies. Structures were optimized at the M062x/may-cc-pVDZ level employing the SMD solvation and Grimme dispersion. Vibrational and rotational contributions to the free energy were taken from these calculations. On these structures, gas phase energies were computed with the CBS-QB3 [18] composite method, without re-optimizing the geometries. On the same structures, free energies of solvation were computed with the SMD model using the M06-2X/6-31G(d) method, without re-optimizing the geometries. The total Gibbs free energy G is thus given by E(gas, CBS-QB3) + ΔG(vib/rot, M062x/may-cc-pVDZ/SMD) + ΔG(solv/SMD, M062x/6-31+G*).

Table S3: List of chemicals, manufacturers, and purities

Compound name	Manufacturer	Purity	Manufacturer Ref.
Phenol	Fluka, Buchs, Switzerland	≥ 99.5%	RA10224
p-methylphenol	Fluka	≥ 99%	GA12831
p-ethylphenol	Aldrich, Steinheim, Germany	99%	E44205
p-isopropylphenol	Aldrich	98%	175404
p-tertbutylphenol	Aldrich	99%	425761
p-chlorophenol	Sigma-Aldrich	≥ 98%	25860
p-bromophenol	Aldrich	99%	B75808
p-cyanophenol	Fluka	≥ 97%	54797
p-formylphenol	Aldrich	98%	144088
p-carboxyphenol	Fluka	98%	54630
p-carboxyphenol	Aldrich	≥ 99%	240141
p-methoxyphenol	Aldrich	99%	M18655
Catechol	Merck, Hohenbrunn, Germany	99%	822261.0250
p-methylcatechol	Merck	98%	821257
p-ethylcatechol	Alfa Aesar, Karlsruhe, Germany	98%	A12048
p-tertbutylcatechol	Merck, Darmstadt, Germany	98%	801987
p-bromocatechol	Tokyo Chemical Industry	> 98%	B2173
p-cyanocatechol	Alfa Aesar	97%	A14738
p-formylcatechol	Aldrich	97%	D108405
p-carboxycatechol	Aldrich	≥ 97%	37580
p-methoxycatechol	Apollo Scientific, Manchester, UK	98%	
2,6-dimethylphenol	Fluka	≥ 99%	41345
2,6-dibromophenol	Fluka	≥ 97%	WB11048
3-bromocatechol	Alfa Aesar	95%	H26925
Hydroquinone	Sigma-Aldrich	≥ 99%	H9003
p-benzoquinone	Fluka	resublimated	12309
2,6-dimethyl-p-benzoquinone	Aldrich	99%	D149705
2,6-dibromo-p-benzoquinone	Indofine Chemical Comp, Hillsborough, NJ, USA	>98%	CS-257
2,6-dimethylhydroquinone	Tokyo Chemical Industry	>98%	D2667
3-methylcatechol	Aldrich	98%	M34006
H_2O_2	Sigma	ppa ≥ 35%	95299
$HOCl/ClO^-$	Sigma	6-14%	13440
NaOH	Merck	≥ 99%	106498
H_3PO_4	Sigma	ppa >= 85%	30417
$NaH_2PO_4*H_2O$	Merck	99-102%	1.06346
$Na_2HPO_4*2H_2O$	Merck	≥ 99.5%	1.06580
Tert-butanol	Sigma	ppa ≥ 99.7%	19460

S1. Second-order rate constants and pK_as of phenols and phenolates.

S1.1 Estimation of unknown second order rate constants and pK_as

Quantum chemical calculations were performed with the Gaussian09 software package. All geometries were optimized at the M05/6-31+G(d) in conjunction with the SMD implicit solvation model. All structures were confirmed as minima by frequency calculations. On these structures, single point energy calculations were performed at the M11/6-311+G** level of theory in cunjunction with the SMD implicit solvation model. For iodine (iodophenols are among the experimental rate constants), the def2-TZVPP basis set was used instead.

pK_a values were computed by evaluating the electronic energy difference

$\Delta E = E(H_3O^+) + E(PhO^-) - E(H_2O) - E(PhOH)$

$pK_a = -\log(\exp(- \Delta E/(R*T)))$

Although using electronic energies instead of Gibbs free energies is not theoretically thorough, we decided to use ΔE instead of ΔG as this yielded a (slightly) better correlation with experimental pK_a values (Figure S1).

To estimate second order rate constants, vertical ionization energies (VIEs) were computed as descriptors. That is, opposed to adiabatic ioniaztion energies, the geometry of the ionized species was computed in the (frozen) geometry of the unionized species. Reported values refer to simple electronic energy differences:

$VIE = E(PhOH^{\cdot+}) - E(PhOH)$ or $VIE = E(PhO^{\cdot}) – E(PhO^-)$

The calculations used the restricted open-shell Kohn-Sham (ROKS) approach. However, unrestricted (UKS) calculations were initially performed, a wavefunction stability analysis was perfomed, and the resulting unrestricted solution was used as a guess for the restricted solution.

Computed VIEs were correlated with experimental second order rate constants (n=35) from von Sonntag and von Gunten [2]. Experimental pK_a values were those of the remainder of the set of phenols used in the present study (n=10). Resulting regression models are shown in Figure S1 and they were used to calculate unknown pK_as and second order rate constants.

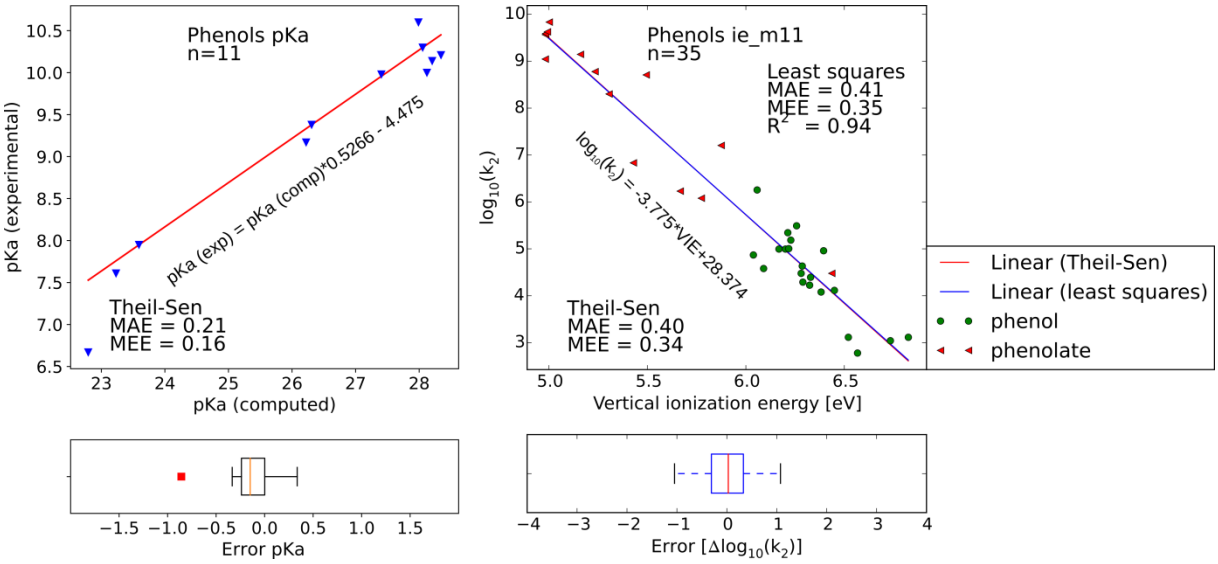

Figure S6: Regression models for pK_a and second order rate constant estimations for the reactions with ozone of phenols/phenolates. The Theil-Sen slope was used; given statistical descriptors are the mean absolute error (MAE) and the median error (MEE).

S1.2 Kinetic treatment of phenol-ozone reactions

The total rate of disappearance of phenol in a second order reaction with ozone is given by

$$-\frac{d}{dt}[PhOH_{tot}] = k(PhO^-)\alpha[PhOH_{tot}][O_3] + k(PhOH)(1-\alpha)[PhOH_{tot}][O_3]$$

where k are second order rate constants for the reactions of phenolate (PhO^-) and phenol (PhOH) with ozone, k_{obs} is the apparent second order rate constant, and $PhOH_{tot}$ refers to the phenol concentration irrespective of speciation. This can be rewritten in terms of degrees of dissociation alpha, equivalent to fractions of the species f:

$$-\frac{d}{dt}[PhOH_{tot}] = k_{obs}[PhOH_{tot}][O_3] = k(PhO^-)[PhO^-][O_3] + k(PhOH)[PhOH][O_3]$$

$$-\frac{d}{dt}[PhOH_{tot}] = \left(\alpha k(PhO^-) + (1-\alpha)k(PhOH)\right)[PhOH_{tot}][O_3]$$

$$\alpha = \frac{1}{1+\frac{[H^+]}{K_a}} = f_{PhO^-}; (1-\alpha) = f_{PhOH}$$

$$k_{obs} = f_{PhO^-}k(PhO^-) + f_{PhOH}k(PhOH)$$

In Table 1 (main text), we report the (percentage) contribution of each species to the apparent rate constant:

$$\%k(PhOH) = \frac{f_{PhOH}k(PhOH)}{k_{obs}}; \%k(PhO^-) = \frac{f_{PhO^-}k(PhO^-)}{k_{obs}}$$

Electronic effects of the ring have two effects: activation will lead to an increase of the pK_a and thus to a decrease of f(PhO^-). As k(PhO-) > k(PhOH), this leads to a decrease in k_{obs}. However, activation also leads to an increase in k(PhO^-) and k(PhOH), which leads to an increase of k_{obs}.

For the upper and lower boundaries given in Table 1 for $\%k_2$ values, we considered an uncertainty of 1xlog(k_2) in both the rate constant of the phenol and the phenolate, and we assumed no uncertainty in the pK_a.

For the calculation of the apparent second order rate constant k_{obs} at pH 7, we did not consider uncertainties in the underlying pK_a and rate data. Experimental data was used whenever available. We note that the outlier in the pK_a regression in Figure S1 (lower left corner) is 2,6-dibromophenol. Its predicted pK_a would amount to 7.5 (instead of the experimental value of 6.67), and the associated k_{obs} value at pH 7 would be reduced to $4.6 \times 10^7 M^{-1}s^{-1}$.

S2. Chromatograms and HRMS data from *p*-methylphenol reaction mixtures.

Figure S2 shows retention times of transformation products from LC-HRMS and HPLC-DAD runs, which use the same column but slightly different elution conditions. As a result, retention times are not the same due to the implementation of differing HPLC equipments and gradients, but as we can clearly assign some of the compounds (TP16/17, TP10, *p*-methylphenol), meaningful comparisons can still be made.

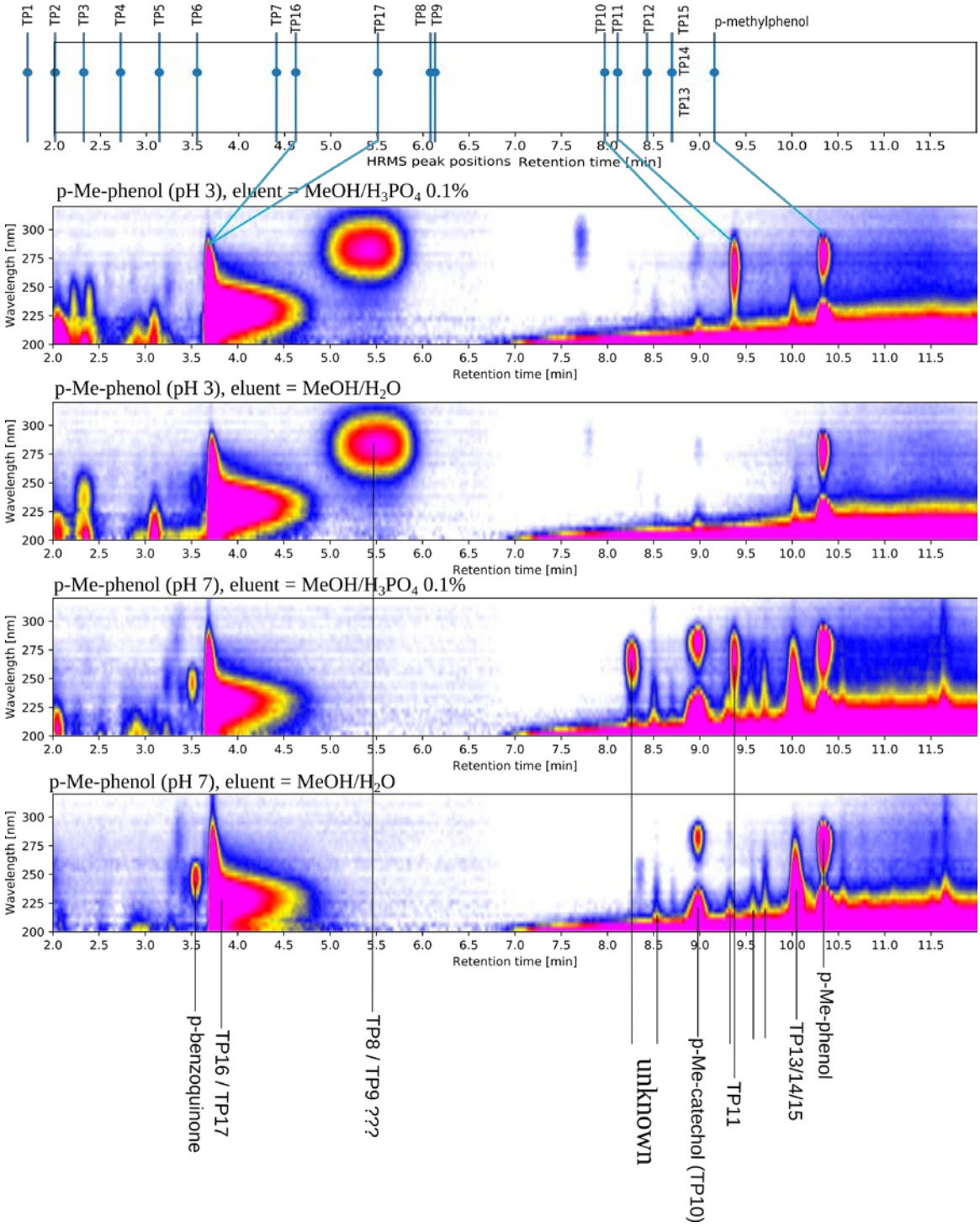

Figure S7.1: Top: LC-HRMS retention times of metabolites found in *p*-methylphenol ozonation reaction mixtures. Bottom: HPLC-DAD chromatograms of *p*-methylphenol ozonation reaction mixtures, elution with either H_2O/MeOH or H_3PO_4 /0.1%/MeOH at pH 3 or pH 7 showcases easily ionizable compounds.

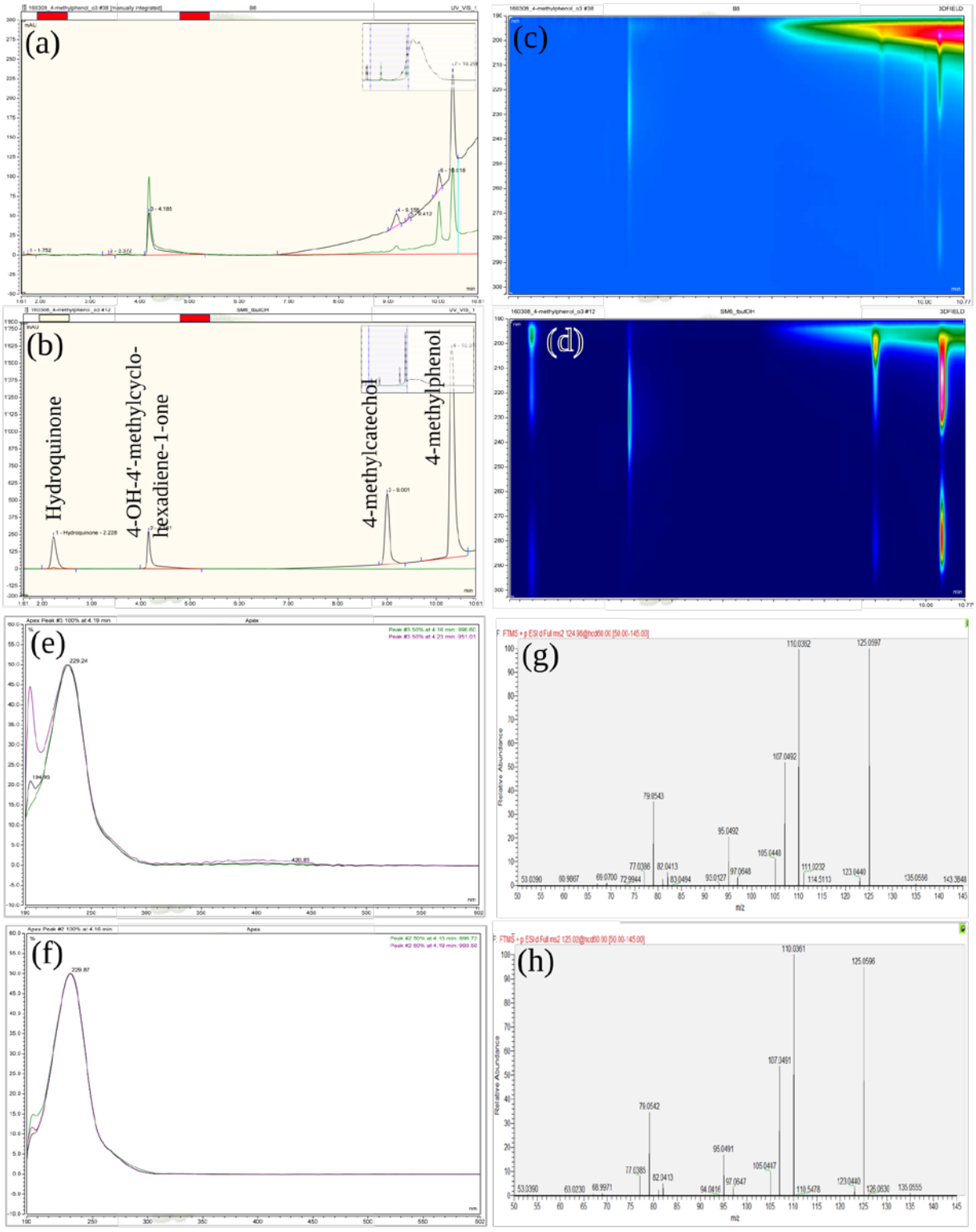

Figure S2.2: Comparison of synthesized standard of *4-hydroxy-4'-methylcyclohexadiene-1-one* with the reaction mixture of *p*-methylcatechol ozonation. HPLC chromatograms at 220 nm of (a) sample and (b) standard mix, 3D chromatograms of (c) sample and (d) standard mix, UV/Vis spectrum at a retention time of 4.2 min of (e) sample and (f) standard mix, MS/MS mass spectra of this peak of (g) sample and (h) standard.

Ozonation experiments were carried out with deuterated parent substances as well. Deuteration pattern in the transformation products, along with absolute MS peak intensities, are shown in Table S2.

Table S4: Properties of HRMS peaks with deuterated *p*-methylphenol. Ring deuteration refers to aromatic deuterons (+4 d in the parent), methyl deuteration to the *p*-methyl-group (+3 d in the parent)

Retention time	Name	Mass shift	Ring deuteration	Methyl deuteration	Intensity (pH 3)	Intensity (pH 7)
1.71	TP1	+3 O	+4 d	+3 d	1.26E+07	3.39E+06
2.01	TP2	+4 O	+3 d	+3 d	6.34E+05	5.23E+06
2.32	TP3	+4 O	+3 d	+3 d	1.09E+06	2.68E+06
2.72	TP4	+2 O	+3 d	+2 d/+3 d	7.52E+06	3.55E+06
3.14	TP5	+3 O	+3 d	+3 d	4.39E+06	6.09E+06
3.55	TP6	+2 O, -2 H	+2 d (40%)/+3 d (60%)	+3 d	2.53E+07	4.75E+07
4.41	TP7	+2 O, -2 H	+3 d	+3 d	2.14E+07	2.24E+07
4.62	TP16	+1 O	+4 d	+3 d	7.73E+07	1.14E+08
5.51	TP17	+1 O, -2 H	+3 d	+3 d	-	2.91E+07
6.08	TP8	+3 O	+4 d	+3 d	8.13E+07	1.86E+06
6.13	TP9	+2 O	+4 d	+3 d	9.42E+05	-
7.97	TP10	+1 O	+3 d	+3 d	2.61E+06	4.14E+07
8.11	TP11	+3 O	+3 d	+3 d	7.25E+06	6.89E+06
8.43	TP12	+1 O, -2 H	+3 d	+2 d	3.49E+06	-
8.7	TP13	+2 O	+3 d (30%)/+4 d (70%)	+3 d	-	2.24E+06
8.7	TP14	+1 O, -2 H	+3 d	+3 d	2.36E+07	4.50E+08
8.7	TP15	+1 O	+4 d	+3 d	-	2.95E+07
9.16	p-methyl-phenol		+4 d	+3 d		

S3. Identification of 4-methyl-*o*-benzoquinone

LC-HRMS data of the *p*-methylphenol reaction mixture at pH 7 indicated that together with the 4-hydroxy-4'-methylcyclohexadiene-1-one, 4-methyl-o-benzoquinone is co-eluting in a very broad peak. Although the given retention times for these transformation products (TP16, TP17) are different, these peaks share the same onset (likely the *t*-BuOH front). In the HPLC-DAD chromatograms, the alleged "mix" of these compounds elutes at 3.7 min (Figure S1). In Figure S3, we show the UV/Vis spectra of different reaction mixtures at 3.7 min: for *p*-methylphenol at pH 3, this is identical to the spectrum of the synthesized standard of 4-hydroxy-4'-cyclohexadiene-1-one, and no absorption can be seen around 400 nm. At pH 7, a weak absorption can be observed around 400 nm. In ozonation experiments of *p*-methylcatechol, the cyclohexadienone band is missing, and the absorption at 400 nm is pronounced (at both pHs). We assign this to the *p*-methyl-*o*-benzoquinone. The same peak is also observed when reacting *p*-methylcatechol with HOCl (Figure S3).

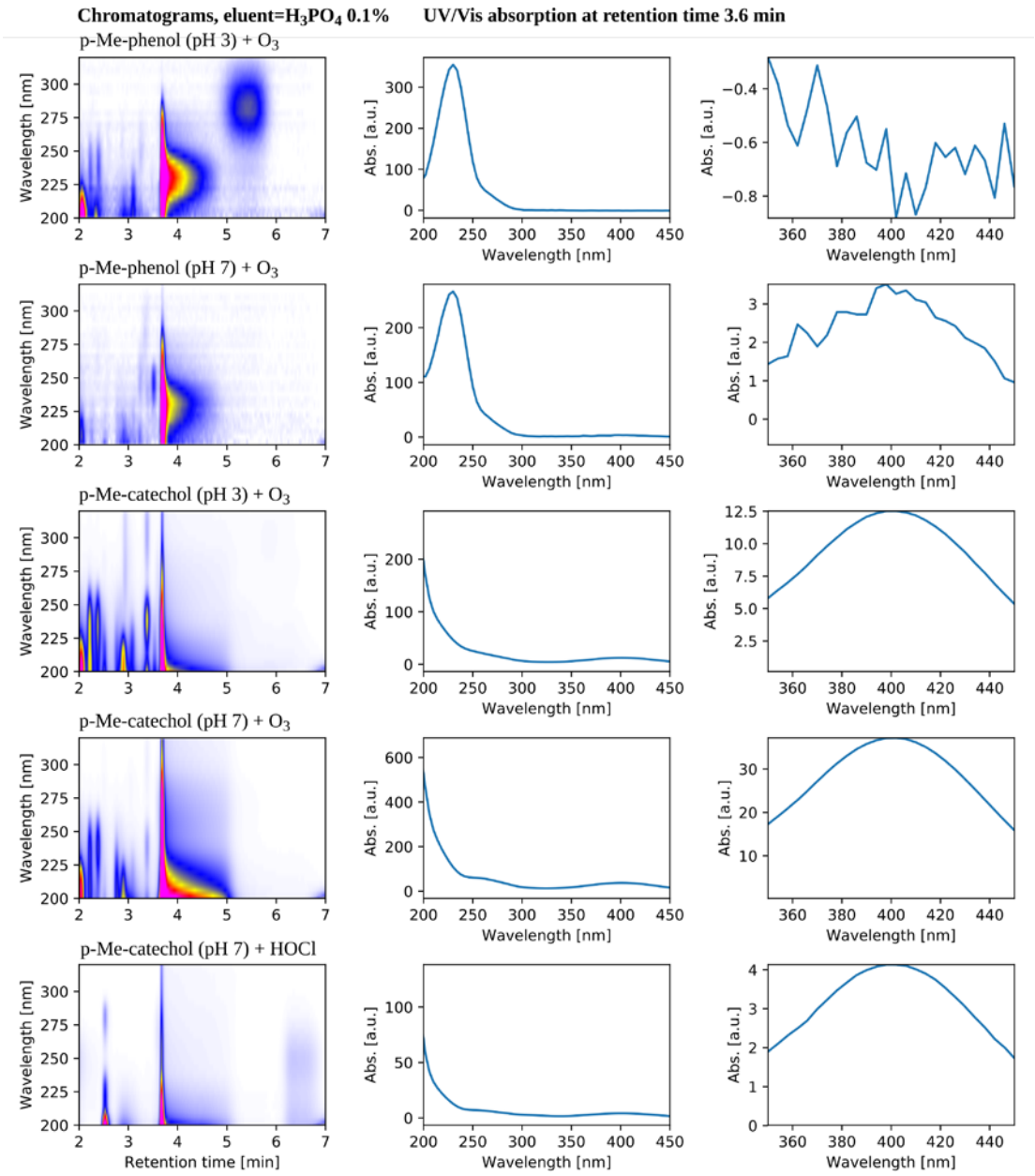

Figure S8: Left: HPLC-DAD chromatograms of *p*-methylphenol and *p*-methylcatechol reaction mixtures with ozone and HOCl as oxidants. Middle: UV/Vis spectra at a retention time of 3.7 min. Right: Zoom on the region around 400 nm.

S4. Hydroquinone formation in the *p*-methoxyphenol reaction mixture

We propose that hydroquinone was formed by the reduction of initially formed *p*-benzoquinone by *p*-methoxycatechol. Quantum chemical calculations indicated a free energy of reaction of 1 kcal/mol, wherefore, this reaction should be thermodynamically feasible within the margin of error of such calculations. We believe the error on the computed free energy of reaction to be rather low: the reaction is homodesmic (meaning that the same types of bonds are present on the reactant and product side, which leads to error cancellation in computed thermodynamics), and also errors in the implicit solvation model should be mostly cancelled out. We repeated the calculations with the CBS-QB3 method (gas phase), to which we added SMD solvation energies, yielding a virtually unchanged result.

We conducted an additional experiment, mixing pure substances *p*-benzoquinone and *p*-methoxycatechol. The chromatogram of this mixture is shown in Figure S4. Of the observed peaks, we can clearly assign those for which standards were available: hydroquinone, *p*-benzoquinone, *p*-methoxycatechol. Thus, it seems reasonable to assume that *p*-benzoquinone was reduced to hydroquinone. This should yield the *o*-quinone, which we identified with the dominant unassigned peak, owing to an absorption band at ~420 nm.

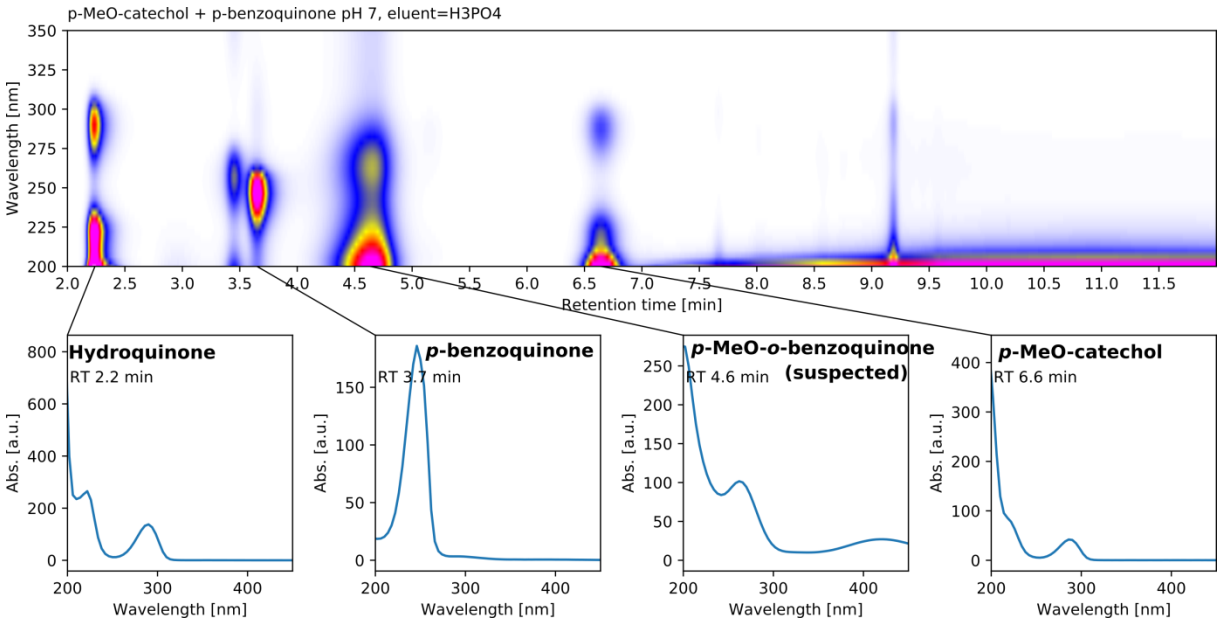

Figure S9: HPLC-DAD chromatogram of a mixture of *p*-methoxycatechol and *p*-benzoquinone (mix of 100 µM solution in phosphate buffer, pH 7). Extracted UV/Vis spectra of known components and presumed *p*-methoxy-*o*-benzoquinone.

S5. Expected post-ozonation dynamics in the presence of nucleophiles

(1) Ozonation of (substituted) phenols yields p benzoquinones and catechols

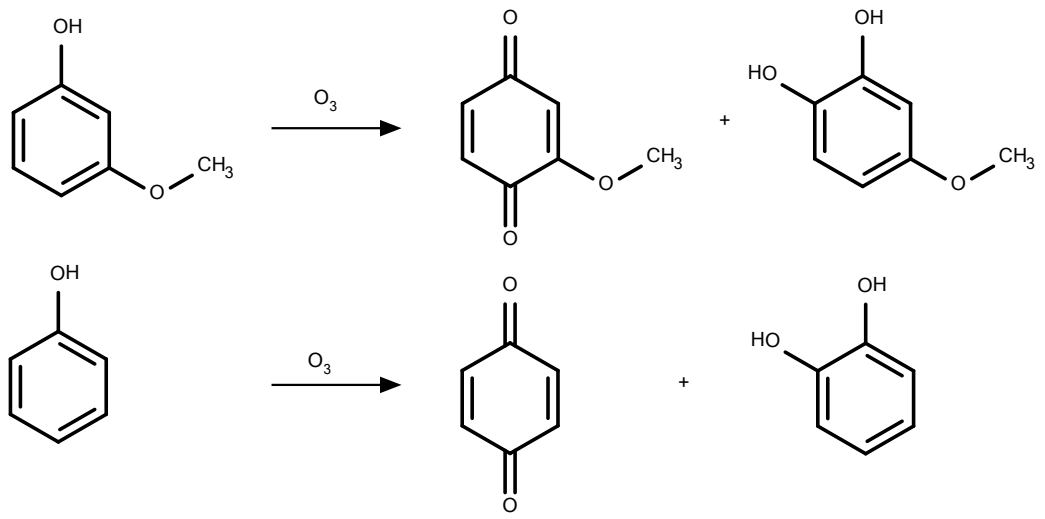

(2) p benzoquinones undergo reductive addition with nucleophiles (thiols, amines, hydroxide)

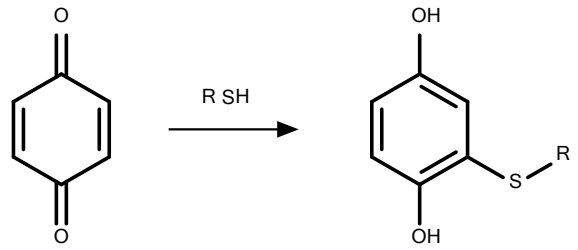

(3) Fast redox equilibria lead to the thermodynamically preferrable benzoquinone/hydroquinone/catechol distribution

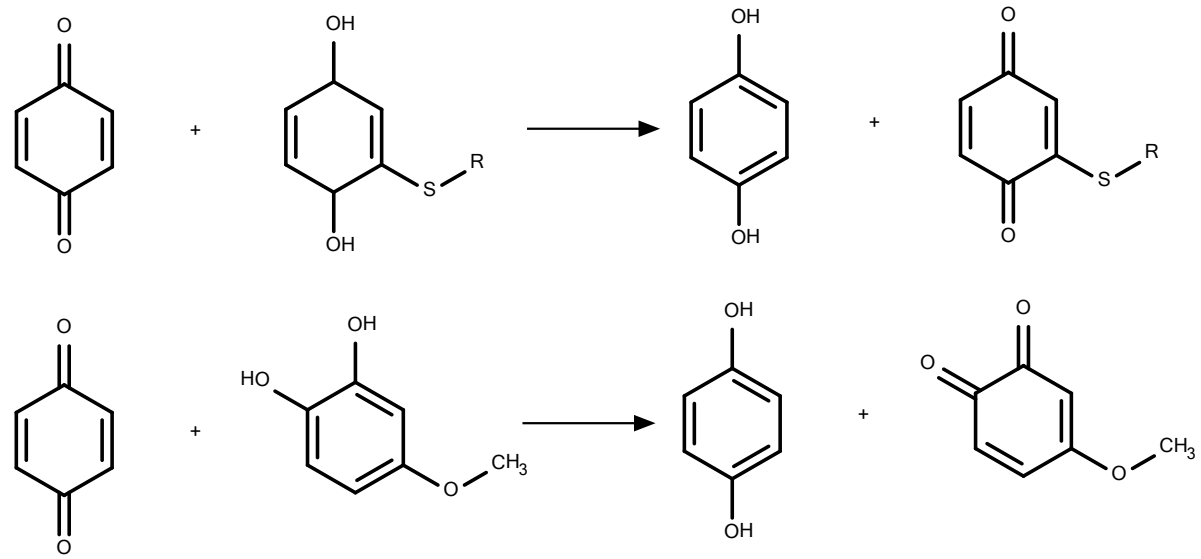

Figure S10: Examples of expected reactions of primary products of ozonation of (substituted) phenols. In biological media (e.g. inside cells), nucleophiles in addition to hydroxide are present (amino groups of amino acids, thiol groups of cysteine moieties of enzymes).

S6. Product yield as a function of specific ozone dose

Batch ozonation experiments were conducted by adding different volumes of room temperature ozone stock to a phenol solution. One experimental series consisted of 7 dosages, adding 1, 1, 2, 2, 5, 5, and 10 mL of ozone stock solution to the phenol solution. In the plots shown below, series conducted on different days with different phenol and ozone stock solutions are shown in different colors.

Where several series are shown, a significant spread of observed yields can be observed. The experiments with the most repetitions are those of phenol at pH 7 and of p-methylphenol at both pH 3 and pH 7.

In ozonation reactions, the yield of transformation products is not independent of the O_3:parent ratios. As products are themselves O_3-reactive (e.g., in the case of catechols, which are more reactive than the parent compounds), the products are consumed with increasing O_3 dose.

A linearly interpolated yield was calculated for each series between the averages of the four data points adjacent to the target ozone dose of 0.5. That is, the two values at the first ozone dose higher than 0.5 were averaged, the two values at the first ozone dose lower than 0.5 were averaged, and a value between these two averages was interpolated.

As there are ≤ 5 independent series, we give the uncertainty as the full range explored by these values. These correspond to deviations from the arithmetic mean of ±6% (p-benzoquinone yield of phenol at pH 7, N=5), +16/-11% (catechol yield of phenol at pH 7, N=5), +10/-16% (cyclohexadienone yield of p-methylphenol at pH 7, N=4), +21/-25% (p-methylcatechol yield of p-methylphenol, pH 7, N=4), +4/-3% (cyclohexadienone yield of p-methylphenol at pH 3, N=4) and +20/-18% (p-methylcatechol yield of p-methylphenol, pH 3, N=4). It is assumed that similar uncertainties can be expected for other parent substances as well. The error bars in Figure 1 (main text) correspond to an uncertainty of the interpolated average of ±6% for p-benzoquinones, +/-15% for cyclohexadienones, and to ±25% for catechols.

Owing coelution of several transformation products in the HPLC-DAD chromatogram, 3-bromocatechol could not unambiguously identified or quantified. The yields shown are best estimates under the assumption that the measured product is in fact 3-bromocatechol.

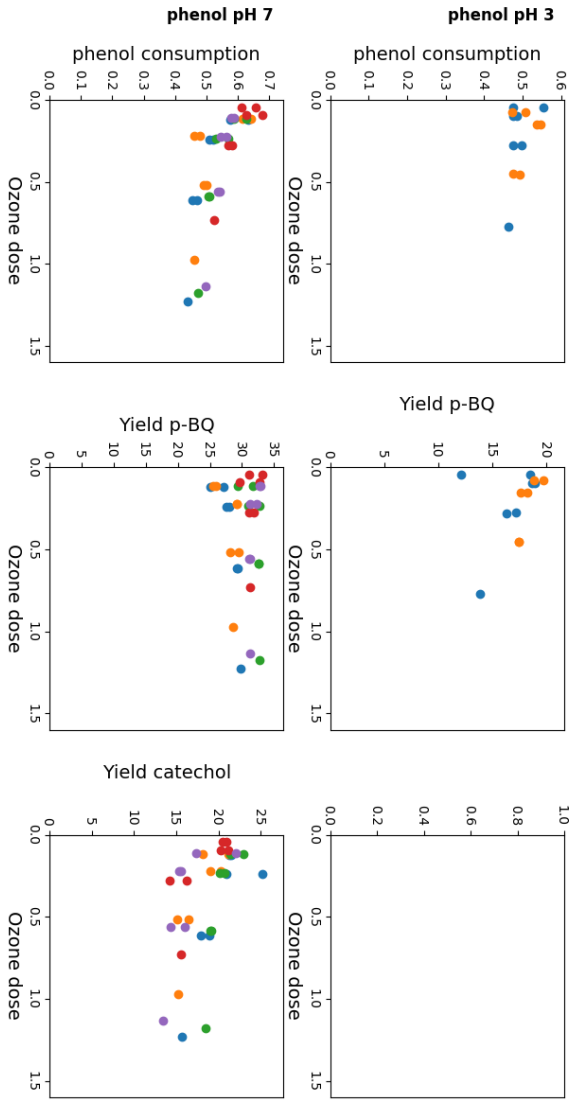

372

373 Figure S6.1: Product yields as a function of specific ozone dose for unsubstituted phenol. Different
374 colors refer to different experimental series (see above). Empty plots indicate that no catechol was
375 detected.

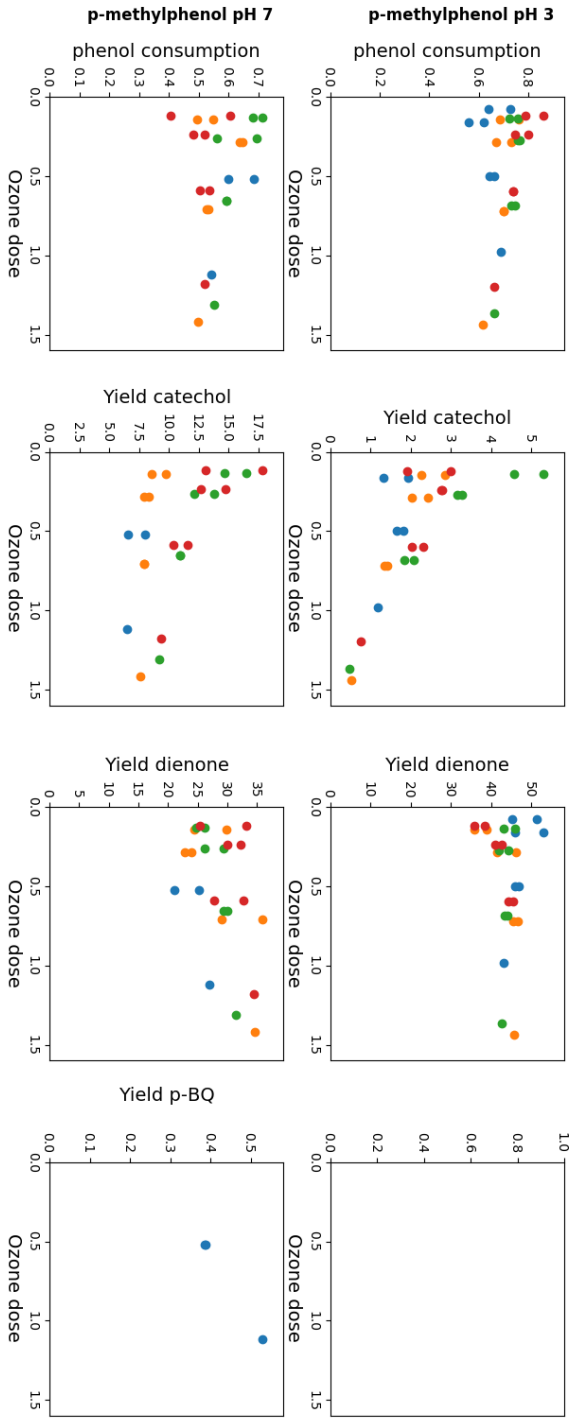

376

377 FigureS6.2: Product yields as a function of specific ozone dose for *p*-methylphenol.

378

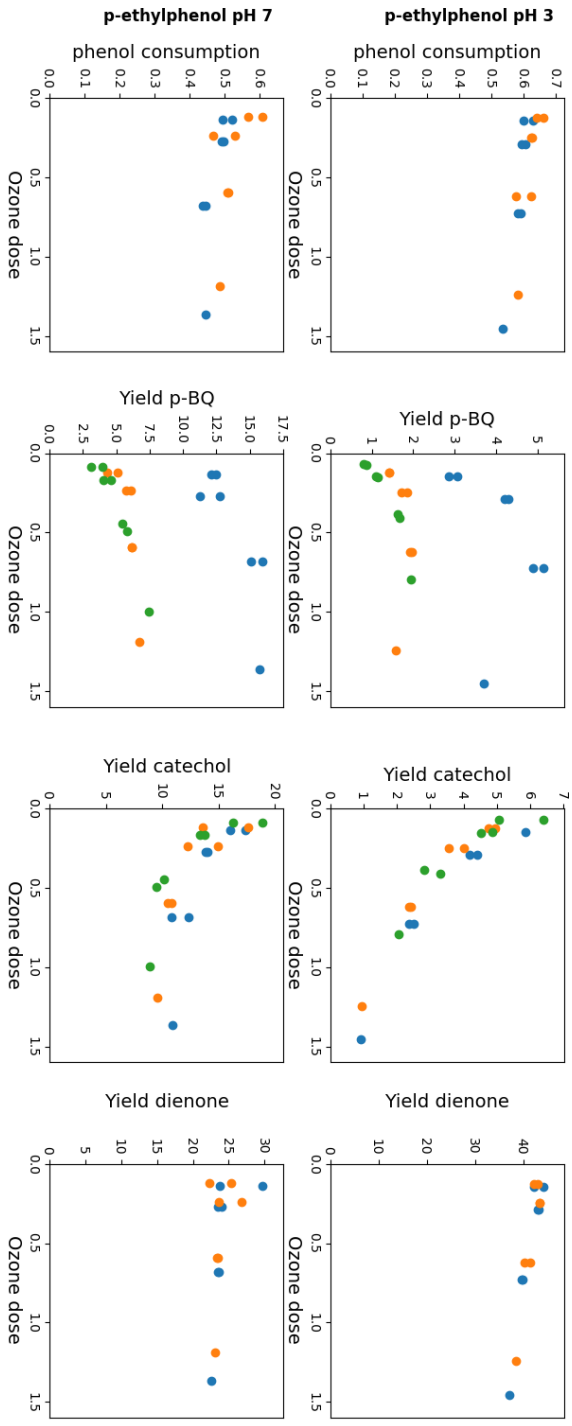

379

380 Figure S6.3: Product yields as a function of specific ozone dose for *p*-ethylphenol.

381

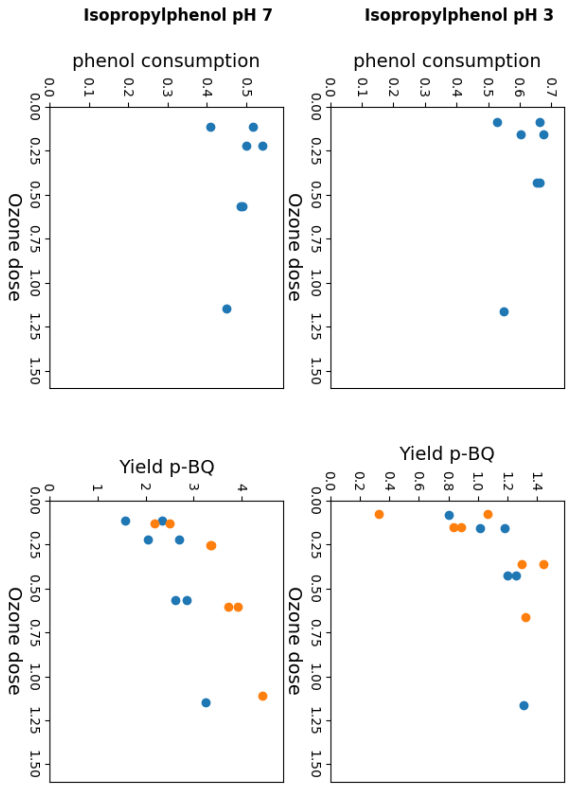

382

383 Figure S6.4: Product yields as a function of specific ozone dose for *p*-isopropylphenol.

384

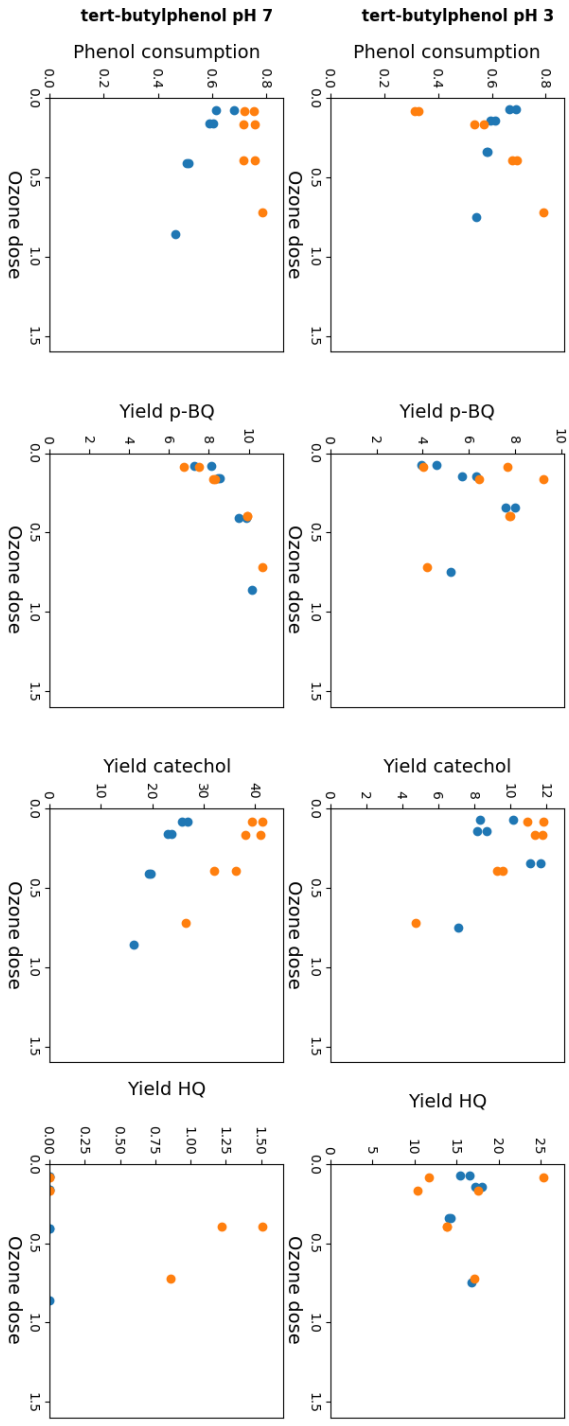

385

386 Figure S6.5: Product yields as a function of specific ozone dose for *p-tert*-butylphenol.

387

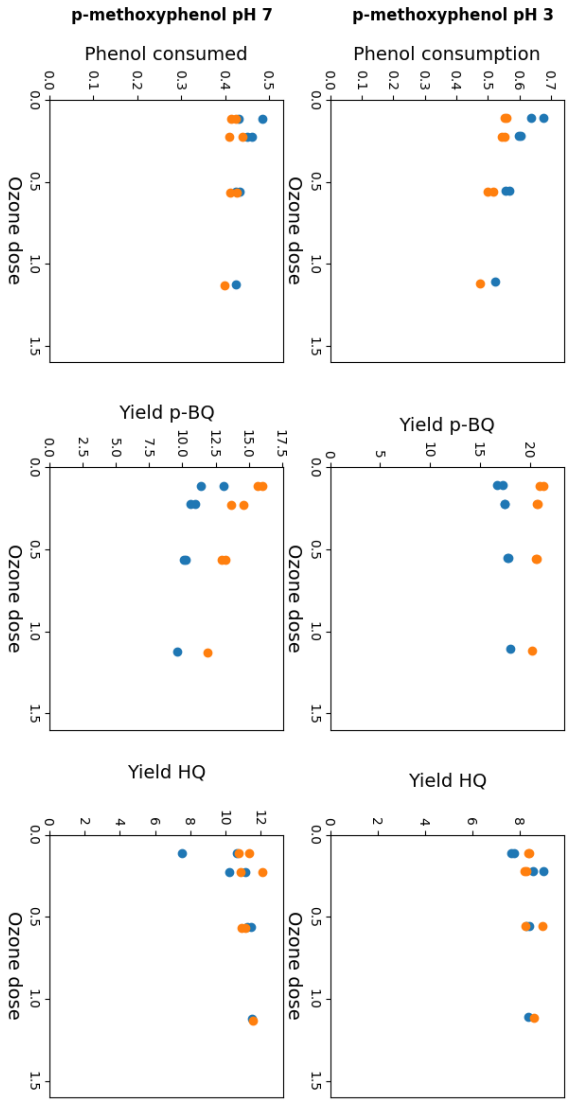

388

389 Figure S6.6: Product yields as a function of specific ozone dose for *p*-methoxyphenol.

390

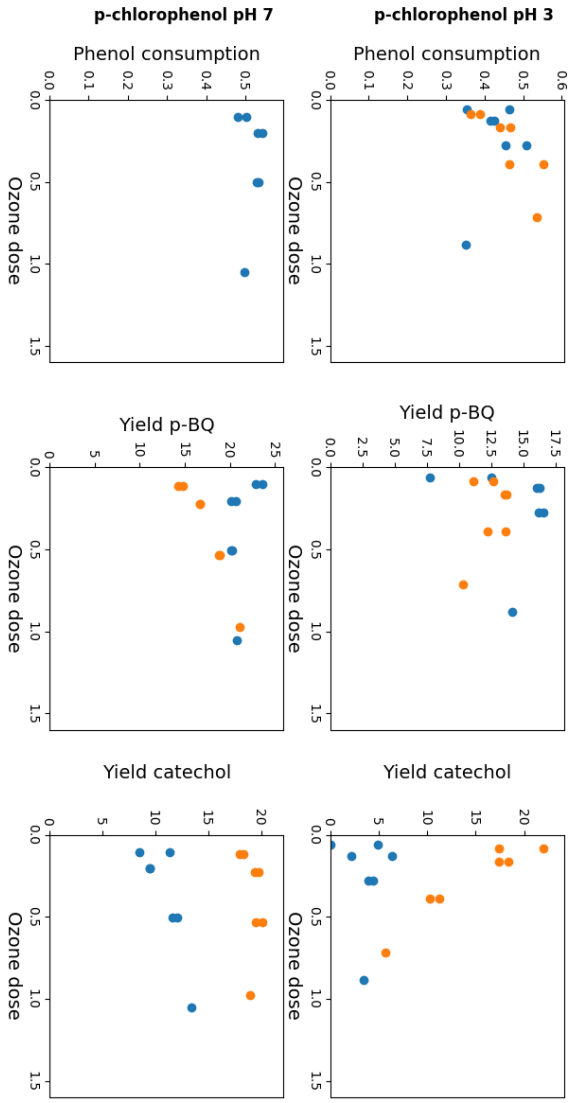

391

392 Figure S6.7: Product yields as a function of specific ozone dose for *p*-chlorophenol.

393

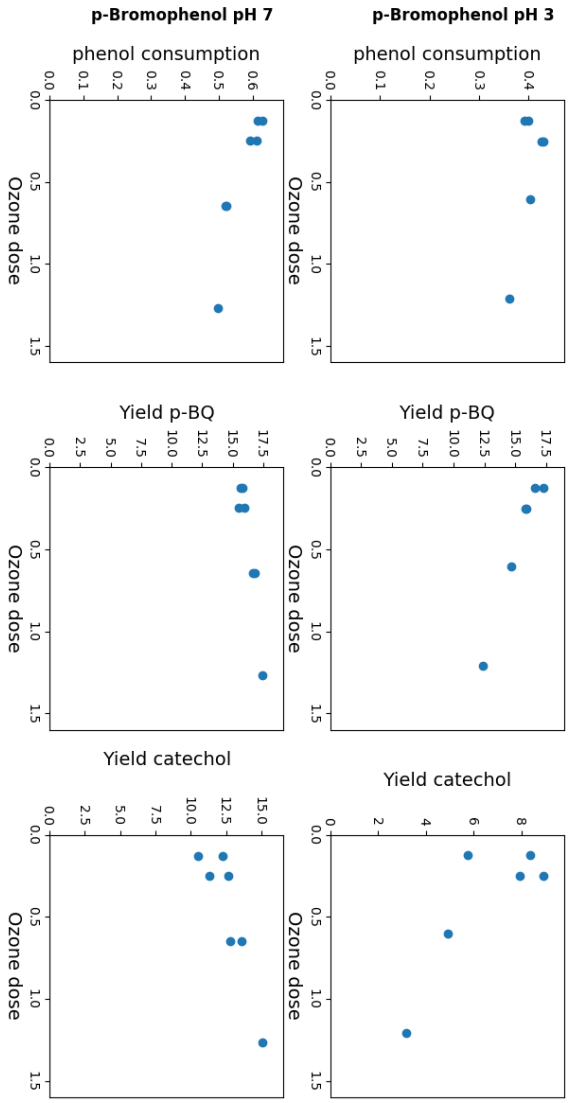

394

395 Figure S6.8: Product yields as a function of specific ozone dose for *p*-bromophenol.

396

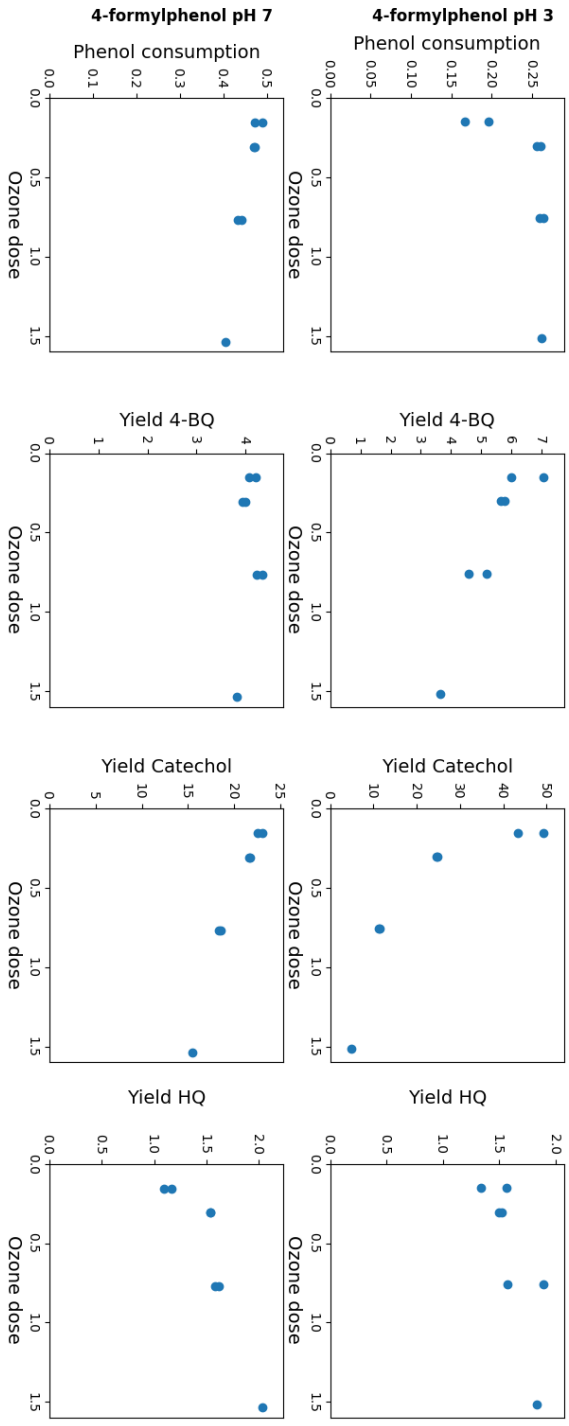

Figure S6.9: Product yields as a function of specific ozone dose for *p*-formylphenol.

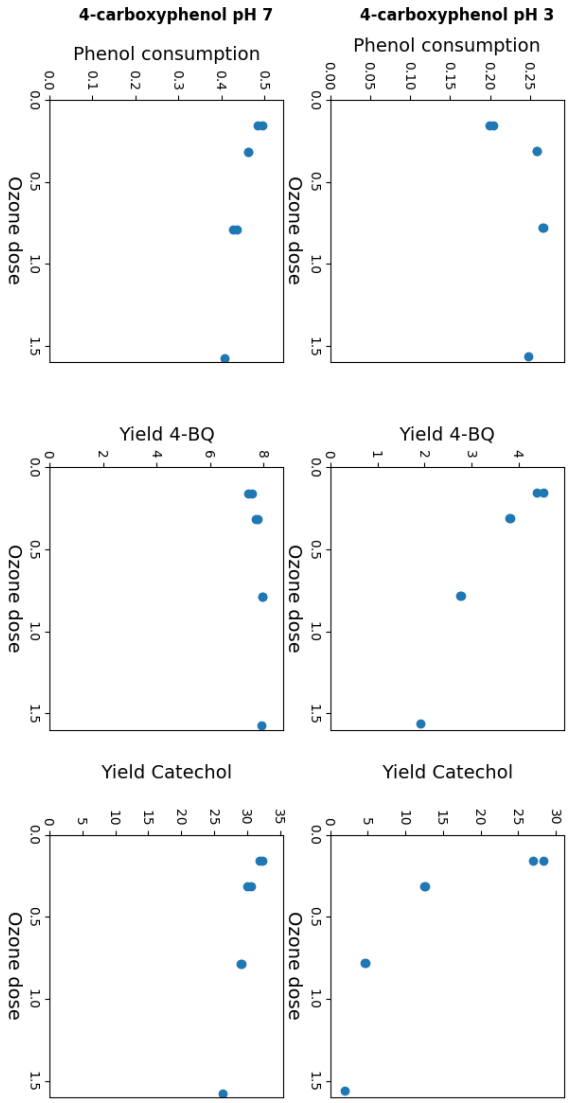

400

401 Figure S6.10: Product yields as a function of specific ozone dose for *p*-carboxyphenol.

402

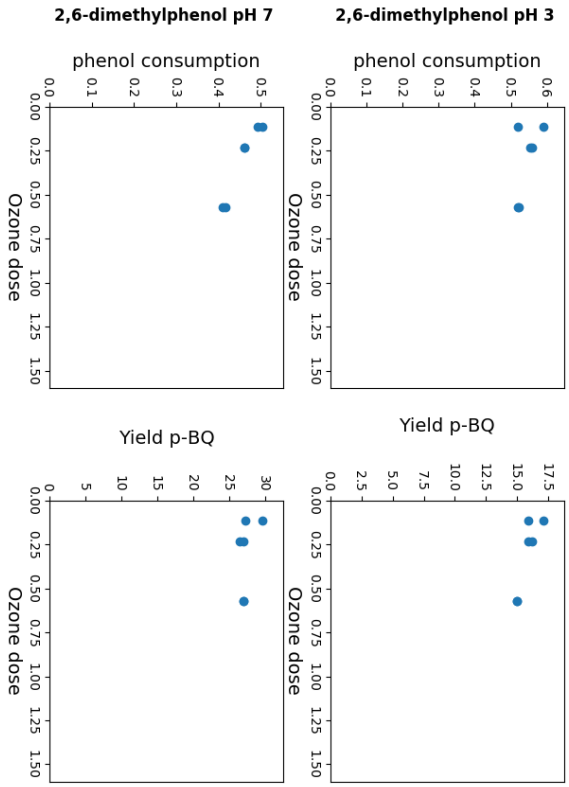

403

404 Figure S6.11: Product yields as a function of specific ozone dose for 2,6-dimethylphenol.

405

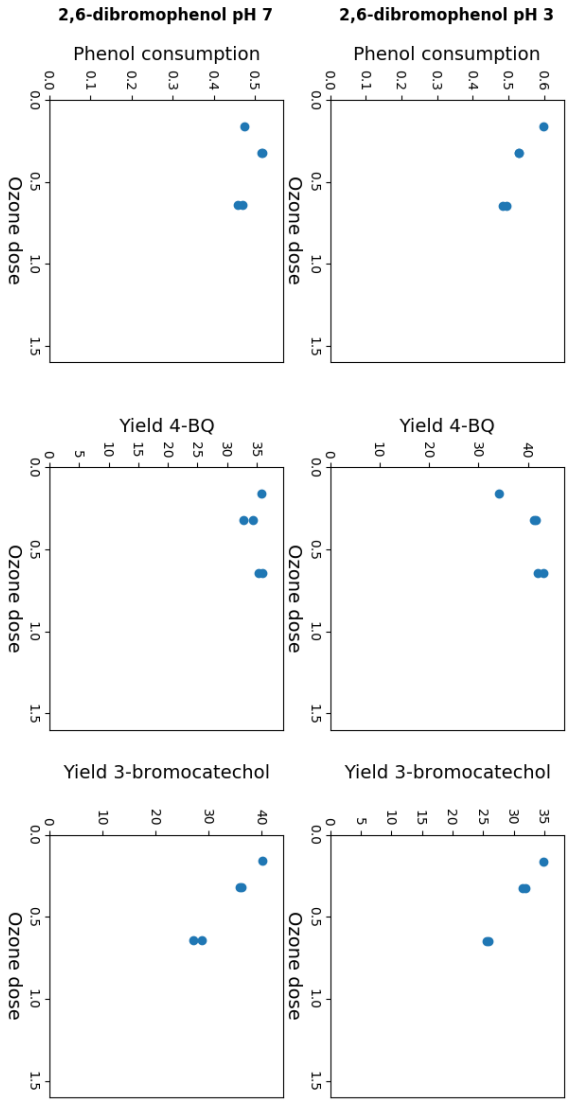

406

407 Figure S6.12: Product yields as a function of specific ozone dose for 2,6-dibromophenol. 3-
408 bromocatechol was not unambiguously identified, owing to overlapping peaks. Given yields are best
409 estimates assuming the correct identity of the transformation product.

410

411

412

413

414

415

S7. Mechanistic discussion

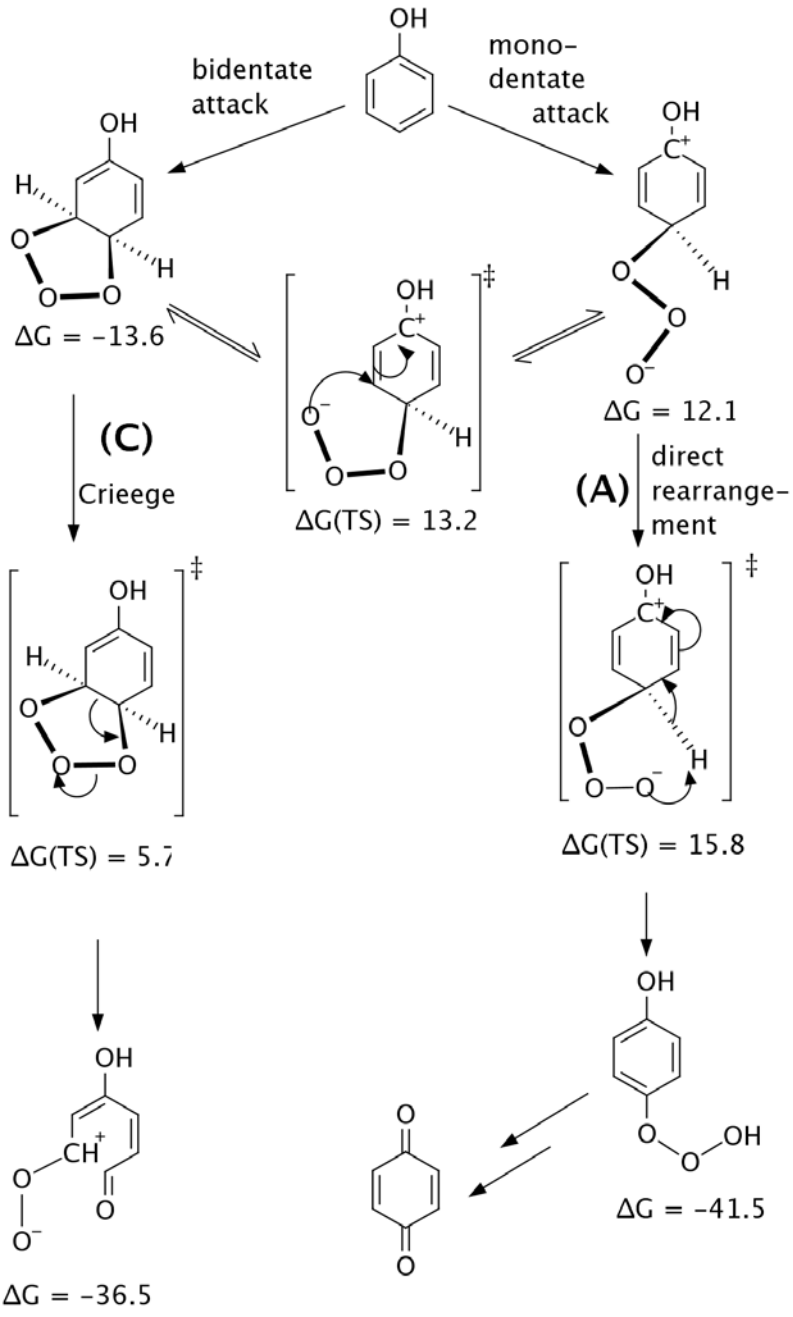

Figure S7.1: Evaluated reaction pathways for neutral phenol. Reported energies are Gibbs free energies (kcal/mol) with respect to separate molecules of ozone and phenol. IRC calculations for transition structures leading to the cyclic ozonide and to the trioxo-species were not successful, presumably because the potential energy surfaces are very flat in these regions.

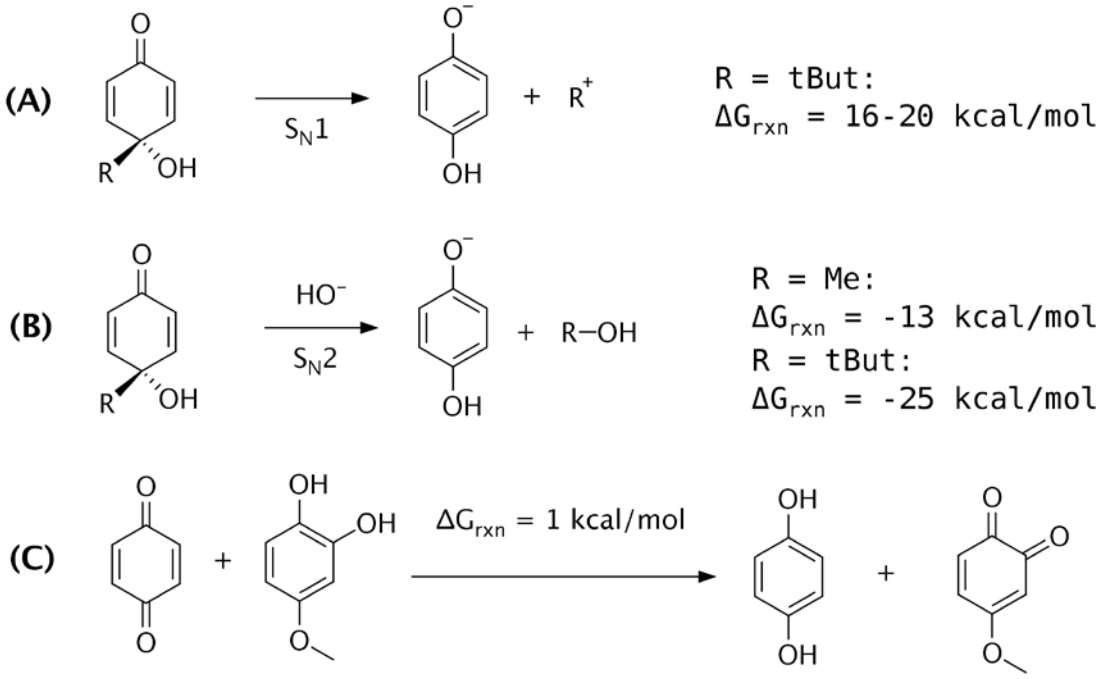

Figure S7.2: Proposed formation pathways of hydroquinone in the reaction mixtures of *p*-tert-butylphenol and *p*-methoxyphenol. Free energies from CBS-QB3 gas phase calculations and SMD implicit solvation energies. Free energies for the S_N1 reaction vary depending on the inclusion of explicit water molecules (not shown).

References

1. Carreño, M.C., M. González-López, and A. Urbano, *Oxidative De-aromatization ofpara-Alkyl Phenols intopara-Peroxyquinols andpara-Quinols Mediated by Oxone as a Source of Singlet Oxygen.* Angewandte Chemie International Edition, 2006. **45**(17): p. 2737-2741.
2. von Gunten, U. and C. von Sonntag, *Chemistry of Ozone in Water and Wastewater Treatment*. 2012: IWA Publishing.
3. Soulard, M., F. Bloc, and A. Hatterer, *Diagrams of Existence of Chloramines and Bromamines in Aqueous-Solution.* Journal of the Chemical Society-Dalton Transactions, 1981(12): p. 2300-2310.
4. M., B.H.U.G.K.G., *Methoden Enzym. Anal. (3. Aufl.)* 1970.
5. Bader, H., V. Sturzenegger, and J. Hoigne, *Photometric-Method for the Determination of Low Concentrations of Hydrogen-Peroxide by the Peroxidase Catalyzed Oxidation of N,N-Diethyl-P-Phenylenediamine (Dpd).* Water Research, 1988. **22**(9): p. 1109-1115.
6. Zhao, Y. and D.G. Truhlar, *The M06 suite of density functionals for main group thermochemistry, thermochemical kinetics, noncovalent interactions, excited states, and transition elements: two new functionals and systematic testing of four M06-class functionals and 12 other functionals.* Theor. Chem. Acc., 2008. **120**(1-3): p. 215-241.

7. Clark, T., et al., *Efficient Diffuse Function-Augmented Basis Sets for Anion Calculations. Iii. The 3-21+G Basis Set for First-Row Elements, Li-F*. Journal of Computational Chemistry, 1983. **4**(3): p. 294-301.
8. Frisch, M.J., J.A. Pople, and J.S. Binkley, *Self-Consistent Molecular-Orbital Methods .25. Supplementary Functions for Gaussian-Basis Sets.* Journal of Chemical Physics, 1984. **80**(7): p. 3265-3269.
9. Krishnan, R., et al., *Self-Consistent Molecular-Orbital Methods .20. Basis Set for Correlated Wave-Functions.* Journal of Chemical Physics, 1980. **72**(1): p. 650-654.
10. Papajak, E., et al., *Perspectives on Basis Sets Beautiful: Seasonal Plantings of Diffuse Basis Functions.* Journal of Chemical Theory and Computation, 2011. **7**(10): p. 3027-3034.
11. Marenich, A.V., C.J. Cramer, and D.G. Truhlar, *Universal Solvation Model Based on Solute Electron Density and on a Continuum Model of the Solvent Defined by the Bulk Dielectric Constant and Atomic Surface Tensions.* Journal of Physical Chemistry B, 2009. **113**(18): p. 6378-6396.
12. Grimme, S., *Semiempirical GGA-type density functional constructed with a long-range dispersion correction.* Journal of Computational Chemistry, 2006. **27**(15): p. 1787-1799.
13. Chai, J.D. and M. Head-Gordon, *Long-range corrected hybrid density functionals with damped atom-atom dispersion corrections.* Physical Chemistry Chemical Physics, 2008. **10**(44): p. 6615-6620.
14. Yamaguchi, K., et al., *A Spin Correction Procedure for Unrestricted Hartree-Fock and Moller-Plesset Wavefunctions for Singlet Diradicals and Polyradicals.* Chemical Physics Letters, 1988. **149**(5-6): p. 537-542.
15. Fukui, K., *The Path of Chemical-Reactions - the Irc Approach.* Accounts of Chemical Research, 1981. **14**(12): p. 363-368.
16. Peverati, R. and D.G. Truhlar, *Improving the Accuracy of Hybrid Meta-GGA Density Functionals by Range Separation.* Journal of Physical Chemistry Letters, 2011. **2**(21): p. 2810-2817.
17. Lee, M., et al., *Development of Prediction Models for the Reactivity of Organic Compounds with Ozone in Aqueous Solution by Quantum Chemical Calculations: The Role of Delocalized and Localized Molecular Orbitals.* Environ Sci Technol, 2015. **49**(16): p. 9925-35.
18. Montgomery, J.A., et al., *A complete basis set model chemistry. VII. Use of the minimum population localization method.* Journal of Chemical Physics, 2000. **112**(15): p. 6532-6542.